Higgs self-coupling measurement prospects in the $b\bar{b}\ell\ell + E_{\mathrm{T}}^{\mathrm{miss}}$ channel at the FCC-hh

Birgit Stapf[1*], Elisabetta Gallo[2*], Kerstin Tackmann[2*], Christophe Grojean[2*], Michele Selvaggi[3*], Angela Taliercio[4*] and Paola Mastrapasqua[5*]

[1]Institut für Experimentalphysik, Universität Hamburg, Hamburg, Germany.
[2]Deutsches Elektronen-Synchrotron DESY, Hamburg, Germany.
[3]CERN, Geneva, Switzerland.
[4]Northwestern University, Evanston, Illinois, USA.
[5]Centre for Cosmology, Particle Physics and Phenomenology (CP3), Université catholique de Louvain, Louvain-la-Neuve, Belgium.

*Corresponding author(s). E-mail(s): birgit.stapf@cern.ch; elisabetta.gallo@cern.ch; kerstin.tackmann@cern.ch; christophe.grojean@cern.ch; michele.selvaggi@cern.ch; angela.taliercio@cern.ch; paola.mastrapasqua@cern.ch;

1 Introduction

The study of Higgs boson pair production is one of the key benchmarks of the scientific program at future colliders. It offers direct experimental access to the Higgs boson trilinear self-coupling and hence to the structure of the scalar potential itself, allowing unprecedented insight into the electroweak symmetry breaking mechanism. The self-coupling modifier κ_λ, defined as the ratio of the measured value of the self-coupling over its Standard Model (SM) predicted value - λ/λ_{SM} - is used to parameterise any deviation from the SM expectations. A precision measurement of κ_λ down to the percent level is a clear goal for future experiments, as at the end of the HL-LHC era the κ_λ precision is expected to reach only around 50% [1]. In the SM, Higgs pair production events in hadron collisions are a rare occurence - with the production cross-section for a Higgs pair in the dominant gluon-gluon fusion mode being three orders of magnitude smaller than that to produce a single Higgs boson [2].

The hadron collider phase of the Future Circular Collider (FCC-hh) is a proton-proton collider operating at a center-of-mass energy of 100 TeV. It is one of the most ambitious projects planned for the rest of this century and offers ample opportunities in the hunt for new physics, both through its direct detection reach as well as through precision measurements. With the large data set of in total 30 ab^{-1} which is envisioned to be collected during the FCC-hh runtime the Higgs self-coupling will be determined down to the percent level.

Previous projections on κ_λ were obtained in [3], where three final states were considered, $b\bar{b}\gamma\gamma$, $b\bar{b}\tau\tau$ and $b\bar{b}b\bar{b}$, achieving a projected sensitivity of 3.4%–7.8% on κ_λ, depending on the assumed detector performance and systematic uncertainties, and driven mainly by the $b\bar{b}\gamma\gamma$ final state. Here a new channel is added, the $b\bar{b}\ell\ell + E_{\mathrm{T}}^{\mathrm{miss}}$ signature, which has as characteristic the presence of missing transverse energy. This final state is thus particularly sensitive to pile-up, which is expected to be $\mathcal{O}(1000)$ at FCC-hh. We assume here that pile-up mitigation algorithms will affect the reconstruction of objects and their momentum or energy resolution similarly to the present LHC configuration. In this context, we use an improved fast simulation and consider two detector scenarios with related object resolutions and efficiencies. The $E_{\mathrm{T}}^{\mathrm{miss}}$ variable is the magnitude of the negative vector sum of transverse momenta of all objects, so that the respective object resolutions are propagated to the $E_{\mathrm{T}}^{\mathrm{miss}}$ resolution.

The $b\bar{b}\ell\ell + E_{\mathrm{T}}^{\mathrm{miss}}$ analysis considers the sum of signals from the $HH \to b\bar{b}WW^* \to b\bar{b}\ell\nu\ell\nu$, $HH \to b\bar{b}\tau\tau \to b\bar{b}\ell\nu\ell\nu$ and $HH \to b\bar{b}ZZ^* \to b\bar{b}\ell\ell\nu\nu$ Higgs pair decays. These decay channels lead to a final state consisting of two b-jets, two charged light leptons (electrons or muons) and missing transverse energy $E_{\mathrm{T}}^{\mathrm{miss}}$ from neutrinos escaping detection. One of the Higgs boson decays can therefore not be fully reconstructed.

By far the dominant background arises from dileptonic decays of top quark pairs, as such events lead to the same final state, but occur with rates that are seven orders of magnitude larger than the $b\bar{b}\ell\ell + E_{\mathrm{T}}^{\mathrm{miss}}$ signal. Additional backgrounds are single Higgs and single top production, the V + jets Drell-Yan process as well as diboson production and the production of a top quark pair together with vector boson(s).

2 Event generation and simulation

Proton-proton collision events at $\sqrt{s}$= 100 TeV using a fast detector simulation with the Delphes framework [4] form the basis of the prospect studies.

2.1 Monte Carlo event generation

Table 1 gives an overview of all the MC samples used for the analysis presented here. For all samples, the hadronisation effects as well as the further decays of intermediate particles, like the Higgs boson, are modeled with Pythia 8 [5]. Unless otherwise specified in the following, the NNPDF 3.0 [6] parton distribution function from the LHAPDF [7] library is used.

The signal consists of gluon-gluon fusion induced double Higgs production events in the decay channels $HH \to b\bar{b}WW^*$, $HH \to b\bar{b}\tau\tau$ and $HH \to b\bar{b}ZZ^*(\to \ell\ell\nu\nu)$, with the $HH \to b\bar{b}WW^*$ channel being the most abundant, due to the large $H \to WW^*$ branching ratio, as given in Table 2. In addition to the baseline $\kappa_\lambda = 1$ signals, which

Process	Cross-section in pb	k-factor
Signals		
$ggHH$, $\kappa_\lambda = 1$	1.13	1.08
$ggHH$, $\kappa_\lambda = 2.4$	0.49	1.08
$ggHH$, $\kappa_\lambda = 3$	0.59	1.08
Backgrounds		
Top quark production		
$t\bar{t} \rightarrow b\ell\nu\bar{b}\ell\nu$	4751	1.74
Wt	4210	1.34
$t\bar{t}t\bar{t}$	2.3	2.10
Vector boson production		
$Z/\gamma*(\rightarrow \ell\ell) + b\bar{b}/c\bar{c}$	293	2.00
$Z/\gamma*(\rightarrow \ell\ell)Z/\gamma*(\rightarrow b\bar{b}/c\bar{c})$	2.3	1.60
Single Higgs production		
ggH	587	3.76
VBF H	84	4.30
$t\bar{t}H$	45	1.22
VH	37	1.32
$t\bar{t}V(V)$		
$t\bar{t}Z$	38	1.68
$t\bar{t}W$	6.6	2.50
$t\bar{t}ZZ$	0.12	1.30
$t\bar{t}WZ$	0.07	2.30
$t\bar{t}WW$	0.78	1.40

Table 1: Overview of signal and background samples.

are used to design and optimize the analysis, signals with $\kappa_\lambda = 2.4$ and 3.0 are also employed in the interpretation of the event rates as a function of κ_λ. All signals are generated with Powheg [8, 9, 10] at next-to-leading order (NLO). The respective cross-sections are scaled to NNLO by means of a k-factor that is independent of κ_λ [11], following [3] and motivated by the studies in [12].

Decay mode	Branching ratio in %
$HH \rightarrow b\bar{b}WW*(\rightarrow \ell\nu\ell\nu)$	2.58
$HH \rightarrow b\bar{b}\tau\tau(\rightarrow \ell\nu\nu\ell\nu\nu)$	0.89
$HH \rightarrow b\bar{b}ZZ^*(\rightarrow \ell\ell\nu\nu)$	0.12

Table 2: Branching ratios of the HH signal decay channels considered in this analysis.

In contrast, all background processes are generated with MadGraph5_aMC@NLO [13, 14] at leading order, with additional jets and higher order corrections applicable as described in the following.

By far the dominant (and most challenging) background to the $b\bar{b}\ell\ell + E_{\mathrm{T}}^{\mathrm{miss}}$ final state is the production of a top-quark pair, $t\bar{t}$, and in particular its dileptonic decay channel, $t\bar{t} \rightarrow b\ell\nu\bar{b}\ell\nu$, as this leads to exactly the same final state as the signal and is therefore an irreducible background. Since the dileptonic $t\bar{t}$ decay is the rarest $t\bar{t}$ mode - occurring in only around 11% of $t\bar{t}$ events - an exclusive sample containing only

$t\bar{t} \to b\ell\nu\bar{b}\ell\nu$ events is used to ensure sufficient MC statistics. Up to two additional jets are included in the $t\bar{t}$ events, and matched between matrix element and parton shower using the MLM-scheme described in [15]. A second contribution involving top quarks arises from the Wt production mode of a single top quark, along with a vector boson. Here, an inclusive sample involving all top quark and boson decays is used, with events containing up to two MLM matched additional jets. Posing only a small contribution due to its smaller cross-section, the production of four top-quarks (in two pairs), $t\bar{t}t\bar{t}$, (without the presence of additional jets) is considered as well. In each case the LO events are normalized to the respective NLO cross-section, using the same k-factors derived for previous FCC-hh Higgs self-coupling studies [3]. Investigations using an inclusive $t\bar{t}$ sample containing all decay modes showed that the contribution of the channels involving at least one hadronic top-quark decay to final states with two b-jets and two isolated leptons is well below 1% , and can therefore be neglected for the exploratory studies presented here. Similarly, the contribution of single top production in the s/t-channel mode was found to be negligible, as these kind of events rarely result in the $b\bar{b}\ell\ell + E_{\mathrm{T}}^{\mathrm{miss}}$ final state. Only 1 in 10^6 events pass the kinematic selection of the analysis presented here, and accordingly the impact on the measurement precision of κ_λ is below 0.1%.

The production of a vector-boson along with jets poses another significant background, since it is very abundant in proton-proton collisions. However, in order to contribute in the $b\bar{b}\ell\ell + E_{\mathrm{T}}^{\mathrm{miss}}$ analysis at least two additional jets need to be present (e.g. from the splitting of an ISR/FSR gluon), and these jets need to either arise from b-quarks, or be mistagged as b-jets while arising from other quark flavours. We therefore focus here on the two main contributors to the $b\bar{b}\ell\ell + E_{\mathrm{T}}^{\mathrm{miss}}$ final state by requiring the presence of a lepton pair, as well as two b- or c-jets: the production of a Z boson along with either a pair of b- or a pair of c-quarks, $Z/\gamma*(\to \ell\ell) + b\bar{b}/c\bar{c}$, and the production of two Z with one decaying to a lepton and the other decaying to a bottom- or charm-quark pair, $Z/\gamma*(\to \ell\ell)Z/\gamma*(\to b\bar{b}/c\bar{c})$. The events considered here are required to have an invariant mass of the lepton pair of at least 10 GeV at generator level. For $Z/\gamma*(\to \ell\ell) + b\bar{b}/c\bar{c}$ the cross-section is corrected to higher orders following the k-factor used in [3], while the $Z/\gamma*(\to \ell\ell)Z/\gamma*(\to b\bar{b}/c\bar{c})$ cross-section is corrected to NNLO (and to include the loop-induced gluon induced production) as derived in [16]. We further assume that mistag rates of light jets at the FCC-hh will be sufficiently small, and thus neglect the contributions of Z bosons with light flavour jets. The background arising from W bosons together with (heavy flavour) jets is not considered - it is found to be negligible in LHC analyses of the $b\bar{b}\ell\ell + E_{\mathrm{T}}^{\mathrm{miss}}$ channel, such as [17].

Additionally, single Higgs production contributes as a background to di-Higgs events. This background is generated at LO, accounting for up to two additional, MLM-matched jets present in the events. For each production mode the respective cross-section is corrected to higher orders using k-factors derived from the most accurate predictions in [18]. Here, all production and decay modes are considered, since several combinations can lead to the signal final state, for example the abundant gluon-gluon fusion induced production with the Higgs decaying to a pair of b-quarks and two non-prompt leptons, $ggH(\to b\bar{b})$, or the top quark pair associated production with the Higgs decaying to leptons and neutrinos, $t\bar{t}H(\to WW \to \ell\nu\ell\nu)$ and the top-quarks decaying hadronically. In the analysis presented here the latter is found to be the main contribution, constituting around 85% of single Higgs events that contain two b-jets as well as an opposite sign pair of isolated leptons. Gluon-gluon fusion induced events form around 12% of single Higgs events passing this selection, while vector boson fusion production (VBF H) and the associated production with a vector boson (VH) pose minor contributions of 2% and 1%. The dedicated kinematic event selection as described in Section 3.1, designed to specifically suppress top-quark contributions, changes this picture however: it is more efficient at rejecting $t\bar{t}H$ events, reducing its relative contribution to around 54%, while ggH events then account for around 40% of single Higgs events that pass the full kinematic event selection.

Last, events in which vector bosons are produced in association with a top-quark pair, $t\bar{t}V(V)$, form a minor background, and are considered in the various combination of top quark pair, W and Z bosons, as listed in Table 1. They are normalized to NLO cross-sections using the k-factors derived for [3].

2.2 Detector simulation and physics objects reconstruction

The FCC-hh will provide proton-proton collision data with a centre of mass energy of 100 TeV, and very high charged particle track multiplicities of $\mathcal{O}(1000)$ average interactions per bunch crossing. This will be experimentally very challenging and require advanced pile-up mitigation methods. Another challenging aspect will be the high energy of the collision products (such as multi-TeV jets that need to be fully contained in a calorimeter) and the larger forward boost of interactions due to the higher centre of mass energy, meaning that a detector coverage of up to $|\eta| \approx 6$ is required.

A reference detector for the FCC-hh has been designed and described in the conceptual design report [19]. It follows the same principles as current LHC general purpose experiments ATLAS and CMS by combining different detector component layers for different purposes and with different technologies, and it is split into a central region (covering the range $|\eta| < 2.5$), and two forward endcaps (expanding the coverage up to $|\eta| < 6$), which are placed at a distance of 10 m from the interaction point. High precision silicon tracking detectors constitute the tracking systems in both central region and endcaps, requiring solenoid magnetic fields of 4T, and Liquid Argon technology is relied on for the electromagnetic calorimeter in both regions as well as the hadronic calorimeter in the forward endcaps. In the central region the hadronic calorimeter uses scintillating tiles with steel and lead absorbers. A muon system employing drift tube technology forms the outermost layer in each region.

This reference detector design is implemented into the Delphes tool, which describes the response of the detector components using parametrisations of the resolution and efficiency functions, and used as the baseline for the studies presented here (called *Scenario II*). Additionally, a more optimistic *Scenario I*, is also studied for comparison, with improved efficiencies and resolutions, as summarized in Table 3. It should be noted that the resolution of the (b-)jets used in this analysis is determined by the performance of the jet clustering, and not by the intrinsic detector resolutions, encoded in the DELPHES scenarios.

Object	Relative momentum resolution Scenario I	Scenario II	Efficiency Scenario I	Scenario II
Electrons	0.4-1%	0.8-3.0%	76-95%	72-90%
Muons	0.5-3%	1.0-6.0%	90-99%	88-97%%
	Medium b-tagging		80-90%	76-86%
	Mistag rates c-jets		10-20%	

Table 3: Ranges of the relative momentum resolutions as well as efficiencies (including reconstruction and identification efficiency) of the relevant objects for the $b\bar{b}\ell\ell + E_{\mathrm{T}}^{\mathrm{miss}}$ analysis, as parameterized in the DELPHES scenarios studied.

In both cases, pile-up is taken into account in the reconstruction through the efficiency and resolution parametrizations, and assumed to affect efficiencies and resolutions of the objects as in the current LHC detectors.

Details on how the fast simulation of the detector response and the reconstruction of physics objects is implemented in DELPHES are given in [4]. Briefly summarizing, DELPHES uses *ParticleFlow* based reconstruction, resolutions and efficiencies are parametrized as functions of the objects transverse momentum p_{T} and pseudorapidity η. The relevant objects for the $b\bar{b}\ell\ell + E_{\mathrm{T}}^{\mathrm{miss}}$ analysis are reconstructed as follows:

- **Electrons** are reconstructed as a combination of information from the tracking system and the electromagnetic calorimeter, with a single momentum resolution and efficiency parametrization accounting for both of these effects. The total electron reconstruction efficiency is the product of the electron tracking efficiency and a separate electron identification efficiency.
- **Muons** are measured precisely by the tracking system, while the dedicated muon chambers provide identification, with a single efficiency parametrization and their momentum resolution obtained from Gaussian smearing. The total muon reconstruction efficiency is the product of the muon tracking efficiency and a separate muon identification efficiency.
- Muons and electrons used in this analysis are required to fulfill **isolation** criteria, by imposing an upper bound of on the isolation variable I, as defined in DELPHES as [4] :

$$I(P) = \frac{\sum\limits_{i \neq P}^{\Delta R < R, p_T(i) > p_T^{\min}} p_T(i)}{p_T(P)} \tag{1}$$

It is thus the ratio of the transverse momentum sum of all objects above a threshold of $p_T^{\min}$ that are found within a cone of ΔR around object P (excluding P itself), over the transverse momentum of P. If the object P is isolated, this variable takes values near 0. Here we use a threshold of $p_T^{\min} = 0.5\,\mathrm{GeV}$ and a cone radius of

$\Delta R = 0.3$. Electrons are considered isolated if they fulfill the criterion $I < 0.1$, while for muons the upper bound on the isolation variable is set at $I < 0.2$.

- **Missing transverse energy** is calculated from the vectorial sum of the transverse momentum component from all particle-flow tracks and calorimeter deposits, so as $E_{\mathrm{T}}^{\mathrm{miss}} = -\sum \vec{p_T}(i)$, where i runs over all visible, reconstructed objects in the event.
- **Jets** are reconstructed by clustering particle-flow objects with the *anti-kt* algorithm [20], with a resolution parameter of $R = 0.4$. Only jets with a transverse momentum of $p_T > 25$ GeV are considered.
- **b-tagging** is applied as a parameterized efficiency function to the subset of reconstructed jets, which can be matched to a generator level b-hadron. Small fake rates for mistagging charm and light jets are included.

The technical implementation of all the above steps is part of the KEY4HEP project [21], which provides a consistent software stack for *all* future collider facilities. In particular, the samples used here are in EDM4HEP format [22]. They are further processed with the FCCANALYSES framework [23].

3 Measuring the Higgs-self coupling modifier in the $b\bar{b}\ell\ell + E_{\mathrm{T}}^{\mathrm{miss}}$ final state

3.1 Event selection and categorization

As an initial step, only events with all expected objects of the final state reconstructed are selected for further analysis: This *pre-selection* requires at least two b-tagged jets, using the medium working point, and at least one opposite sign lepton pair of either same (SFOS = ee or $\mu\mu$) or different flavour (DFOS = $e\mu$). In case more than one such lepton pair is found, the one with the highest total p_{T} is selected. Both leptons in the pair are required to be isolated - first by fulfilling the isolation selection described in Section 2.2, as well as by being geometrically separated from the selected b-jets, by imposing $\Delta R_{l,b} > 0.4$. Only leptons with a transverse momentum of $p_T > 10$ GeV are selected, while for jets the threshold is $p_T > 25$ GeV, as implemented in the DELPHES scenarios. Moreover, a veto on hadronic τ decays is applied to ensure this analysis remains orthogonal to studies of the hadronic $b\bar{b}\tau\tau$ final states. With this, the $t\bar{t} \to b\ell\nu\bar{b}\ell\nu$ background alone is five orders of magnitude larger than the expected signal. It is therefore clear, that further, strong background suppression is necessary to make a measurement of the Higgs self-coupling in this final state possible.

For this purpose, the specific expected kinematics of the Higgs pair production signal are exploited. Figure 1 illustrates an example of an ideal, expected signal event: Two Higgs bosons are produced at rest (from gluon-gluon fusion, in the absence of additional radiation), and therefore recoil against each other. One of them decays into a pair of b-quarks, and the other for example into two W bosons, which further decay into an electron or muon and the corresponding neutrino. These further decays are boosted due to the recoil between the two Higgs bosons.

Thus, we can make use of the angles within and invariant masses of the different decay systems to select signal-like topologies:

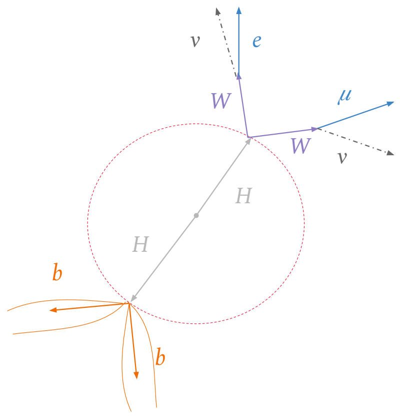

Fig. 1: Illustration of the expected kinematics of an ideal Higgs pair production signal event.

- In the $H \to b\bar{b}$ decay, an invariant mass of the two b-jets, m_{bb}, near the Higgs mass is expected. Figure 2a shows the m_{bb} distributions of signal and backgrounds. Furthermore, the angular distance between two b-jets, ΔR_{bb}, shown in Figure 2b is small, since the $H \to b\bar{b}$ decay is boosted, as described above.
- Similarly, we can exploit the invariant mass of the lepton pair, $m_{\ell\ell}$, as well as the angular distance within this pair, $\Delta R_{\ell\ell}$, shown in Figures 2c and 2d. However, due to the presence of the neutrinos these variables do not fully reconstruct the $H \to \ell\ell + E_{\mathrm{T}}^{\mathrm{miss}}$ decay, and the azimuthal angle between lepton pair and missing transverse energy, $\Delta\phi(\ell\ell, E_T^{\mathrm{miss}})$, shown in Figure 2e is also considered to improve signal to background separation.
- A more complex variable that captures the kinematics of the full HH system is exploited is the $H_{\mathrm{T2}}^{\mathrm{ratio}}$. It is defined as the ratio of the scalar sum of the transverse momenta of the $H \to b\bar{b}$ and $H \to \ell\ell + E_{\mathrm{T}}^{\mathrm{miss}}$ systems, over the scalar sum of all Higgs decay products in the final state:

$$H_{\mathrm{T2}}^{\mathrm{ratio}} = \frac{|\vec{E}_{\mathrm{T}}^{\mathrm{miss}} + \vec{p}_{\mathrm{T}}^{\,ll}| + |\vec{p}_{\mathrm{T}}^{\,bb}|}{E_{\mathrm{T}}^{\mathrm{miss}} + |p_{\mathrm{T}}(l_1)| + |p_{\mathrm{T}}(l_2)| + |p_{\mathrm{T}}(b_1)| + |p_{\mathrm{T}}(b_2)|} \quad (2)$$

  For the signal, where the $H \to b\bar{b}$ and $H \to \ell\ell + E_{\mathrm{T}}^{\mathrm{miss}}$ systems are in balance, this variable is expected to take values near one, whereas this is not the case for background events where the final state objects are more uniformly distributed in the transverse plane, as seen in Figure 2f.

Table 4 summarizes the event selection and categorization, and provides the exact selection thresholds used for each variable. A comparison of the performance of the event selection between signal and the dominant background, $t\bar{t} \to b\ell\nu\bar{b}\ell\nu$, is given in Table 5. The efficiency of the pre-selection is the same for signal and background, and here a significantly limiting factor is the isolation criterion for the leptons. Studying the lepton isolation efficiency in signal events, it was found to be around 60% for

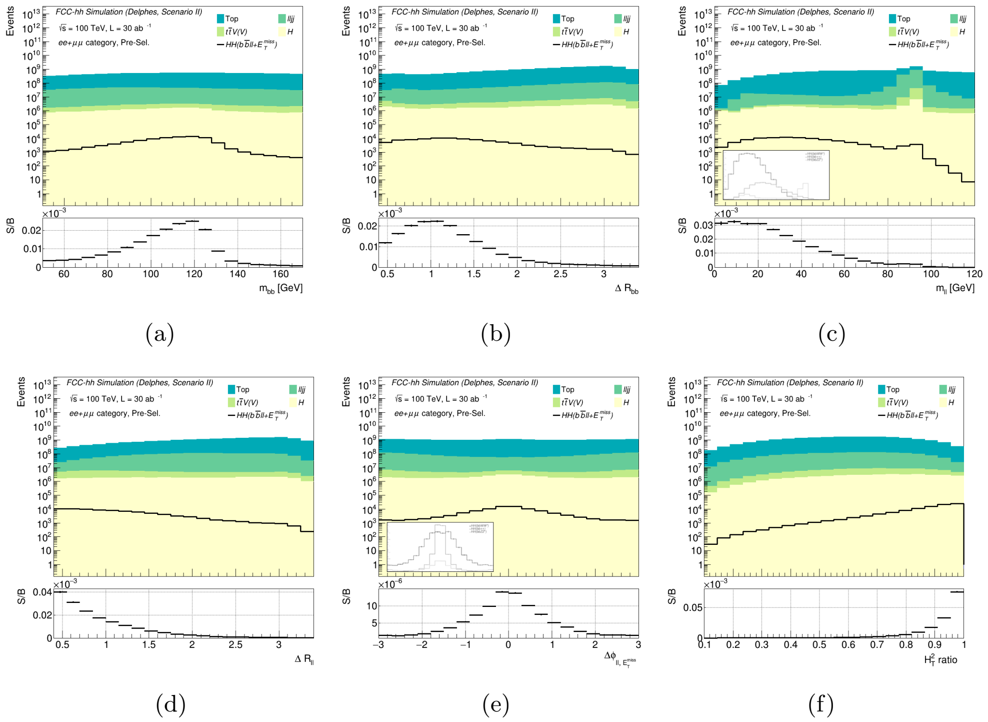

Fig. 2: Distributions of the kinematic variables exploited for the event selection, in pre-selected $ee + \mu\mu$ events, for signal and backgrounds: a) The invariant mass of the two b-jets, m_{bb}. b) The angular distance between the two b-jets, ΔR_{bb}. c) The invariant mass of the selected lepton pair, $m_{\ell\ell}$. d) The angular distance between the two leptons, $\Delta R_{\ell\ell}$. e) The angle between the lepton pair and the missing transverse energy, $\Delta\phi(\ell\ell, E_T^{\text{miss}})$. f) The so called $H_{\text{T2}}^{\text{ratio}}$, as defined in Equation 2. The inlays in c) and e) show the same distributions separately for the different signal channels.

electrons and 75% for muons per lepton, with the main effect coming from the isolation variable selection as defined in Equation 1, and not the requirement for the leptons to be separated from the b-jets. Hence, this analysis could further gain in sensitivity by defining an optimizied isolation requirement with improved efficiency for di-Higgs signal events.

With the kinematic selection a little less than half of the signal events are retained, while nearly 99% of the $t\bar{t} \to b\ell\nu\bar{b}\ell\nu$ background contribution is suppressed. Nonetheless, with this selection a signal-to-background ratio, $S/\sqrt{B}$, considering only the $t\bar{t} \to b\ell\nu\bar{b}\ell\nu$ background, of only around 4 is achieved.

In order to improve further, a dedicated variable to suppress $t\bar{t}$ is employed additionally: the minimum average invariant mass of the lepton and b-jet pairs, $m_{\ell b}^{\text{reco}}$. This variable is used e.g. by the top-quark mass measurement in the dileptonic $t\bar{t}$ channel

	DFOS	Analysis category SFOS, no Z-peak	SFOS, on Z-peak
Main signals	$b\bar{b}WW^*$, $b\bar{b}\tau\tau$	$b\bar{b}WW^*$, $b\bar{b}\tau\tau$	$b\bar{b}ZZ^*$, $b\bar{b}\tau\tau$
Selection variable		Criterion	
Lepton pair	$e\mu$	ee or $\mu\mu$	ee or $\mu\mu$
Number of b-jets		≥ 2	
m_{bb}		85 - 105 GeV	
ΔR_{bb}		< 2	
$\Delta R_{\ell\ell}$		< 1.8	
$H_{\mathrm{T2}}^{\mathrm{ratio}}$		> 0.8	
$m_{\ell b}^{\mathrm{reco}}$		> 150 GeV	
$\Delta\phi(\ell\ell, E_T^{\mathrm{miss}})$	< 2		< 1.2
$m_{\ell\ell}$	10 - 80 GeV		81 - 101 GeV
$\Delta\phi(\ell\ell, E_T^{\mathrm{miss}})$-categories	< 1.2 ("low") and $1.2 - 2.0$ ("high")		-

Table 4: Summary of the event selection and categorization.

with ATLAS [24]. It is defined as:

$$m_{\ell b}^{\mathrm{reco}} = \min\left(\frac{m_{l_1 b_1} + m_{l_2 b_2}}{2}, \frac{m_{l_2 b_1} + m_{l_1 b_2}}{2}\right) \tag{3}$$

where $m_{l_i b_j}$ indicates the invariant mass of the specific combination of lepton i with b-jet j. Since there are two leptons and two b-jets each, there are two possible ways to pair them into two top-decay candidates and for $m_{\ell b}^{\mathrm{reco}}$ the combination leading to the minimum average invariant mass is chosen. Figure 3 shows the $m_{\ell b}^{\mathrm{reco}}$ distributions in signal and backgrounds, in particular comparing the signal shape to that of $t\bar{t} \to b\ell\nu\bar{b}\ell\nu$ events after the kinematic event selection is applied. While in the latter case, the $m_{\ell b}^{\mathrm{reco}}$ distribution peaks below the top-quark mass as expected, it takes larger values for the signal, offering good further separation power. Table 5 reports the impact of selecting only events above a threshold of 150 GeV: the $t\bar{t} \to b\ell\nu\bar{b}\ell\nu$ background is suppressed by an additional order of magnitude in this way, such that the approximate signal-to-background ratio with respect to this background (more than) doubles.

	Sig. acc. in %	$t\bar{t}$ acc. in %	$S/\sqrt{B}$
Pre-selection	15	15	1.03
Kin. selection	44	1.2	4.28
Kin. sel + $m_{\ell b}^{\mathrm{reco}} > 150$ GeV	22	0.07	8.93

Table 5: Performance of the different stages of event selection across all analysis categories. Relative acceptances with respect to the previous selection stage are given, and $S/\sqrt{B}$ is calculated considering only the $t\bar{t} \to b\ell\nu\bar{b}\ell\nu$ background, but the sum of all signal decay channels.

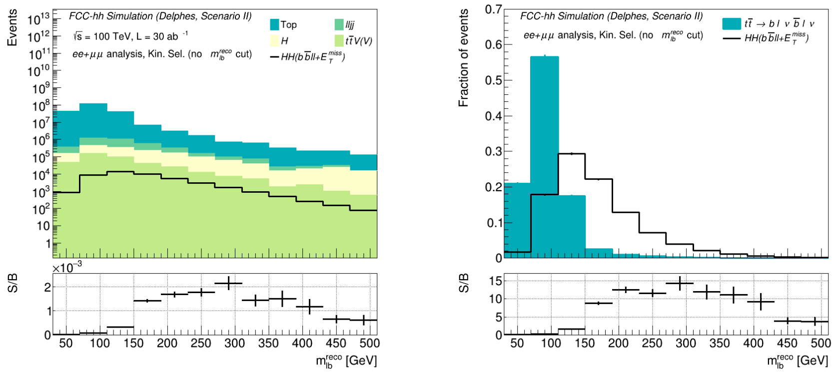

(a) (b)

Fig. 3: Distributions of the $m_{\ell b}^{\mathrm{reco}}$ variable, as defined in Equation 3. In (a) shown for all backgrounds and normalized to the respective cross-section and luminosity and in (b) only for the main signal, $HH \to b\bar{b}WW^* \to b\bar{b}\ell\nu\ell\nu$, and background, $t\bar{t}$, processes, normalized to unit area.

As can be seen in the inlays in Figures 2c and 2e, the $m_{\ell\ell}$ and $\Delta\phi(\ell\ell, E_T^{\mathrm{miss}})$ distributions differ between the different signals, and are therefore used to categorize events. After splitting the events between DFOS and SFOS lepton pairs, the SFOS pairs are further split in a "no Z-peak" and an "on Z-peak" category, by selecting events where $m_{\ell\ell}$ is near the Z boson mass. In the SFOS, on Z-peak category the dominant signal process is then the $HH \to b\bar{b}ZZ^* \to b\bar{b}\ell\ell\nu\nu$ process, although it has the smallest branching fraction, leading to this category having the lowest sensitivity. Since the azimuthal angle between lepton pair and missing transverse energy, $\Delta\phi(\ell\ell, E_T^{\mathrm{miss}})$, takes larger values in the $HH \to b\bar{b}WW^* \to b\bar{b}\ell\nu\ell\nu$ signal when compared to the $HH \to b\bar{b}\tau\tau \to b\bar{b}\ell\nu\ell\nu$ signal, the events in the "no Z-peak" categories are further split into "low" and "high" $\Delta\phi(\ell\ell, E_T^{\mathrm{miss}})$ categories, in order to maximize sensitivity.

3.2 Extracting the Higgs self-coupling modifier

Table 6 gives an overview of the expected number of signal and background events at the FCC-hh for an integrated luminosity of 30 ab^{-1}, after the event selection and categorization as described above. In the most sensitive categories, $S/\sqrt{B}$ values of around 5 are achieved.

To improve the sensitivity to κ_λ further, a binned likelihood based on the distributions of the *pseudo-transverse mass*, m_{T2}, is constructed. This variable, as defined in [25] and [26], is able to capture the full HH decay, by predicting the invisible mass contribution from the neutrinos. Here the C++ code provided in [27] is used to calculate the m_{T2}. As inputs for the two visible momenta the total summed 4-vectors of the two b-jets and the two-leptons are used, together with $E_{\mathrm{T}}^{\mathrm{miss}}$ and assuming a mass of 0 for the invisible particles involved in the decay. The resulting distributions in all

Process	Events at 30 ab^{-1}, FCC-hh scenario II in category				
	DFOS		SFOS, no Z-peak		SFOS, on Z-peak
	Low $\Delta\phi(\ell\ell, E_T^{\text{miss}})$	High $\Delta\phi(\ell\ell, E_T^{\text{miss}})$	Low $\Delta\phi(\ell\ell, E_T^{\text{miss}})$	High $\Delta\phi(\ell\ell, E_T^{\text{miss}})$	All
Signal	1.58E+04	1.87E+03	1.75E+04	1.95E+03	1.86E+03
Top	8.75E+06	2.23E+06	9.20E+06	2.11E+06	3.93E+06
Vector boson	1.45E+05	5.06E+01	3.84E+05	2.29E+05	8.11E+06
Single Higgs	4.11E+05	3.49E+04	4.72E+05	4.51E+04	3.39E+05
$t\bar{t}V(V)$	7.11E+04	1.80E+04	6.99E+04	1.41E+04	8.89E+05
Total Background	9.38E+06	2.28E+06	1.01E+07	2.40E+06	1.33E+07
$S/\sqrt{B}$	5.16	1.24	5.50	1.26	0.51

Table 6: Total number of expected events per process in each category after applying the kinematic event selection.

categories are shown in Figure 4. It is clear that exploiting these distributions in a binned fit improves signal to background separation, and therefore the sensitivity.

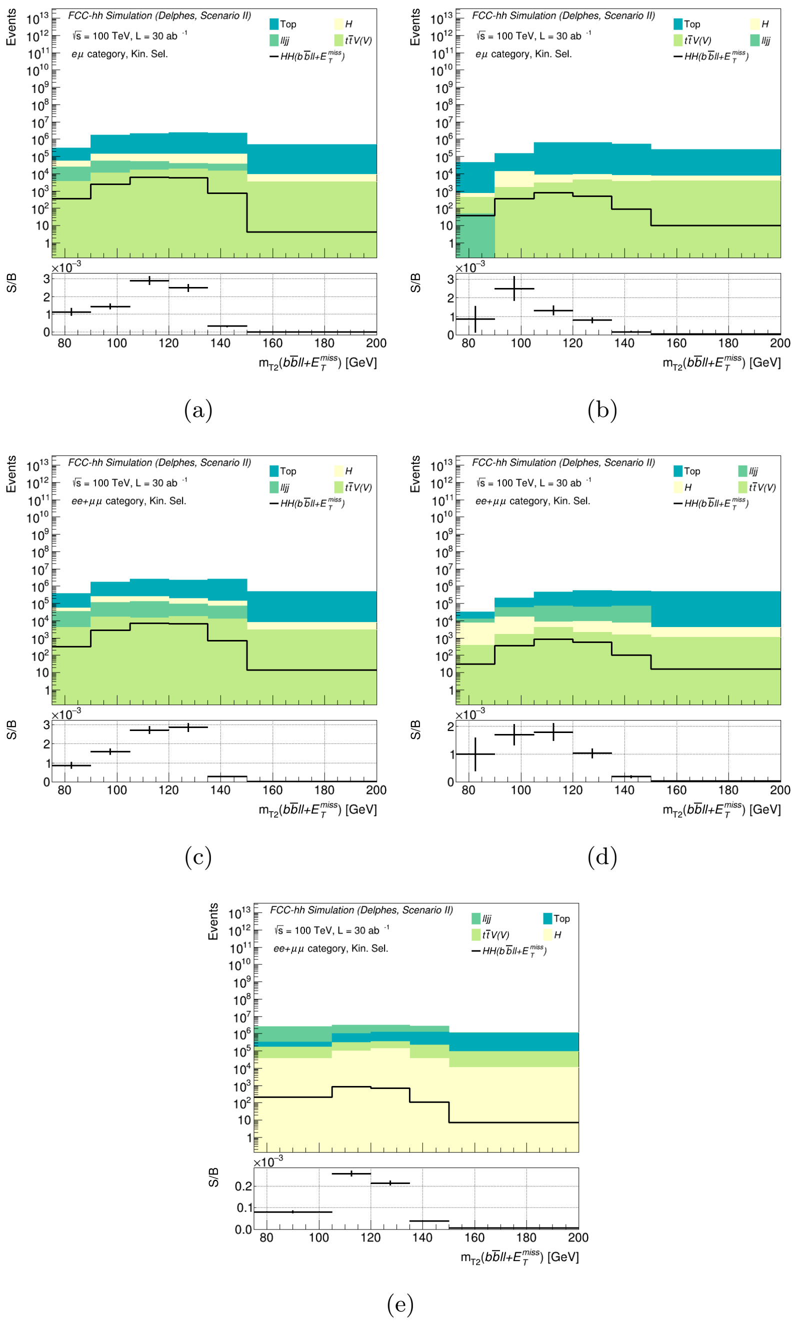

Fig. 4: Distributions of the stransverse mass, m_{T2}, after event selection in the different analysis categories: a) DFOS, low $\Delta\phi(\ell\ell, E_T^{\mathrm{miss}})$ category, b) DFOS, high $\Delta\phi(\ell\ell, E_T^{\mathrm{miss}})$ category, c) SFOS, no Z and low $\Delta\phi(\ell\ell, E_T^{\mathrm{miss}})$ category, d) SFOS, no Z and high $\Delta\phi(\ell\ell, E_T^{\mathrm{miss}})$ category and e) SFOS, on Z-peak category.

This binned fit is performed using the statistical tool COMBINE [28], and following the asymptotic approximation [29]. To extract the Higgs self-coupling modifier κ_λ from the di-Higgs events, the dependence of the di-Higgs production cross-section on κ_λ is parameterised as a function of the event rates for signals with $\kappa_\lambda = 1.0, 2.4, 3.0$. All other Higgs couplings are fixed to their SM values, and in particular no κ_λ dependence or uncertainties are assumed on the involved branching ratios.

3.3 Results and systematic uncertainty benchmarks

The determination of the Higgs self-coupling modifier κ_λ is performed for three different benchmarks of systematic uncertainties, as listed in Table 7. While the two different DELPHES scenarios studied already account for the effect of varying reconstruction and identification efficiencies of the b-jets and leptons, uncertainties are applied for these as well, since the efficiencies are usually measured from data, and MC is corrected to this with limited precision.

The systematic uncertainties considered follow what was done in previous FCC-hh studies [3], assuming for example that the large $t\bar{t}$ and V + jets backgrounds will be measured in data control regions with high precision. The uncertainties are considered as impact on the event rates, not on the kinematic distributions of the process they apply to.

Source of uncertainty	Syst. 1	Syst. 2	Syst. 3	Applies to
b-jet ID / b-jet	0.5%	1%	2%	Signals, MC bkgs.
Lepton ID / lepton	0.5%	1%	2%	Signals, MC bkgs.
Luminosity	0.5%	1%	2%	Signals, MC bkgs.
Signal cross-section	0.5%	1%	1.5%	Signals, MC bkgs.
Data-driven bkg. est.	-	1%	1%	V + jets
Data-driven bkg. est.	-	-	1%	$t\bar{t}$

Table 7: Overview of systematic uncertainties considered.

With these systematic uncertainty benchmarks, as well the detector simulation scenarios described in Section 2, the expected precision on the Higgs self-coupling modifier κ_λ is extracted from the binned likelihood fit described above, as shown in Figure 5. Five different cases are studied: 1) The most optimistic case, using the "idealized" detector scenario I and no systematic uncertainties and 2-5) More realistic cases, using the baseline detector scenario II with no systematic uncertainties, as well as with each of the three different systematic uncertainty benchmarks from Table 7.

Case	$\delta\kappa_\lambda$ (68% CL)
Scen I, stat. only	22.4%
Scen II, stat. only	25.8%
Scen II, syst. 1	30.7 %
Scen II, syst. 2	36.1 %
Scen II, syst. 3	42.7 %

Table 8: Expected, averaged precision on the Higgs self-coupling modifier κ_λ, at 68%confidence level.

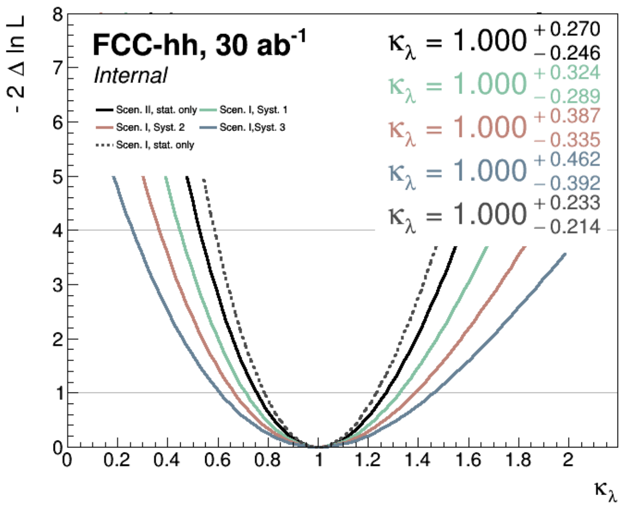

Fig. 5: Expected likelihood scans as a function of κ_λ with the different assumptions on detector performance and systematic uncertainties.

At 68% confidence level, the expected precision on κ_λ ranges from 22.4% in the most optimistic case 1, to 42.7% for the systematic uncertainty scenario 3 and the baseline detector performance, as reported in Table 8. Here, the average of the upper and lower uncertainty are given. The asymmetric behaviour of the likelihood functions with respect to κ_λ is explained by the fact that in the SM, the production cross-section of Higgs pair events as a function of κ_λ exhibits a minimum beyond 1, at around 2.5 - there is therefore a point at $\kappa_\lambda > 2.5$ at which the production cross-section takes the same value as for $\kappa_\lambda = 1$. Using the event rates alone this point can thus not be distinguished from the $\kappa_\lambda = 1$ case, and the shape of the invariant mass of the di-Higgs system, m_{HH}, is needed to provide sensitivity in this respect. The $b\bar{b}\ell\ell + E_T^{\text{miss}}$ analysis however does not achieve this, as the final state can not be fully reconstructed due to the missing transverse energy, leading to the sensitivity for values of $\kappa_\lambda > 1$ being lower than that for values $\kappa_\lambda < 1$ and therefore the likelihood asymmetries seen in Figure 5.

4 Conclusion

An analysis of the prospects of the Higgs self-coupling measurement at the FCC-hh is presented, by investigating the $b\bar{b}\ell\ell + E_{\mathrm{T}}^{\mathrm{miss}}$ final state. The $b\bar{b}\ell\ell + E_{\mathrm{T}}^{\mathrm{miss}}$ channel is a good benchmark for signatures with genuine $E_{\mathrm{T}}^{\mathrm{miss}}$, which are particularly sensitive to pile-up. The precision achievable on the self-coupling modifier κ_λ with this final state ranges from 22% at 68% CL with the most optimistic detector scenario and without systematic uncertainties, to 35% with a more realistic detector scenario and an intermediate set of systematic uncertainties.

Potential improvement for this analysis lies (primarily) in designing a more efficient isolation selection for the signal leptons, as the standard procedure following Delphes was found to disregard a significant fraction of signal events.

While the $b\bar{b}\ell\ell + E_{\mathrm{T}}^{\mathrm{miss}}$ channel is not competitive compared to other channels achieving higher resolution, like the $b\bar{b}\gamma\gamma$ final state and the hadronic decay modes of $b\bar{b}\tau\tau$, a precision of few percent on κ_λ will be possible only by combining several channels and by designing the detectors to achieve the best performance for this measurement.

Acknowledgements

E.G., C.G., B.S. and K.T. acknowledge support by the Deutsche Forschungsgemeinschaft (DFG, German Research Foundation) under Germany's Excellence Strategy – EXC 2121 "Quantum Universe" – 390833306. This work has been partly supported by the Future Circular Collider Innovation Study (FCCIS) project, that has received funding from the European Union's Horizon 2020 research and innovation programme under grant No 951754.

References

[1] ATLAS collaboration, https://cds.cern.ch/record/2802127.
[2] B.D. Micco, M. Gouzevitch, J. Mazzitelli and C. Vernieri, *Reviews in Physics* **5** (2020) 100045.
[3] M.L. Mangano, G. Ortona and M. Selvaggi, *EPJC* **80** (2020) 1030.
[4] J. De Favereau, C. Delaere, P. Demin, A. Giammanco, V. Lemaitre, A. Mertens et al., *JHEP* **02** (2014) 057.
[5] T. Sjöstrand, S. Mrenna and P. Skands, *Computer Physics Communications* **178** (2008) 852.
[6] R.D. Ball, V. Bertone, S. Carrazza, C.S. Deans, L. Del Debbio, S. Forte et al., *JHEP* **2015** (2015) .
[7] A. Buckley, J. Ferrando, S. Lloyd, K. Nordström, B. Page, M. Rüfenacht et al., *EPJC* **75** (2015) .
[8] P. Nason, *JHEP* **11** (2004) 040.
[9] S. Frixione, P. Nason and C. Oleari, *JHEP* **11** (2007) 070.
[10] S. Alioli, P. Nason, C. Oleari and E. Re, *JHEP* **06** (2010) 043.
[11] M. Grazzini, G. Heinrich, S. Jones, S. Kallweit, M. Kerner, J.M. Lindert et al., *JHEP* **05** (2018) 059.

[12] S. Amoroso, P. Azzurri, J. Bendavid, E. Bothmann, D. Britzger, H. Brooks et al., *arXiv* (2020) [2003.01700].
[13] J. Alwall, R. Frederix, S. Frixione, V. Hirschi, F. Maltoni, O. Mattelaer et al., *JHEP* **07** (2014) 079.
[14] R. Frederix, S. Frixione, V. Hirschi, D. Pagani, H.-S. Shao and M. Zaro, *JHEP* **07** (2018) 185.
[15] M.L. Mangano, M. Moretti, F. Piccinini and M. Treccani, *JHEP* **2007** (2007) 013–013.
[16] M.L. Mangano, G. Zanderighi, J.A.A. Saavedra, S. Alekhin, S. Badger, C.W. Bauer et al., , 1607.01831.
[17] ATLAS Collaboration, *Journal of High Energy Physics* **2024** (2024) .
[18] R. Contino, D. Curtin, A. Katz, M.L. Mangano, G. Panico, M.J. Ramsey-Musolf et al., , 1606.09408.
[19] FCC collaboration, *EPJST* **228** (2019) 755.
[20] M. Cacciari, G.P. Salam and G. Soyez, *Journal of High Energy Physics* **2008** (2008) 063–063.
[21] P. Fernandez Declara et al., *PoS* **EPS-HEP2021** (2022) 844.
[22] "*EDM4hep data model*." https://edm4hep.web.cern.ch/.
[23] "*FCCAnalyses framework*." https://github.com/HEP-FCC/FCCAnalyses.
[24] ATLAS Collaboration, *Physics Letters B* **761** (2016) 350.
[25] C. Lester and D. Summers, *Physics Letters B* **463** (1999) 99.
[26] A. Barr, C. Lester and P. Stephens, *Journal of Physics G: Nuclear and Particle Physics* **29** (2003) 2343.
[27] "MT2 / Stransverse Mass / Oxbridge Kinetics Library ." https://www.hep.phy.cam.ac.uk/~lester/mt2/.
[28] CMS collaboration, , 2404.06614.
[29] G. Cowan, K. Cranmer, E. Gross and O. Vitells, *The European Physical Journal C* **71** (2011) .